DIRECT NUMERICAL SIMULATION OF TRIPLE FLAMES BY USING 2-D REACTION-DIFFUSION MANIFOLD TABULATION METHOD

by

Hai Xiang ZENG[a], Ping WANG[b*], Qian YU[a], Meenatchidevi MURUGESAN[b], Linsong JIANG[b], and Prashant SHROTRIYA[a]

[a] School of Energy and Power Engineering, Jiangsu University, Zhenjiang, Jiangsu, China
[b] Institute for Energy Research, Jiangsu University, Zhenjiang, Jiangsu, China

Original scientific paper
https://doi.org/10.2298/TSCI190909198Z

The characteristics of partially-premixed flames is investigated by simulating a series of triple flames with different variations of chemical equivalent ratio. A 2-D reaction-diffusion manifold chemistry tabulation method is employed in the simulation and the results are compared with the CH_4-air 19-step chemical reaction mechanism. The performance of these two mechanisms is then assessed by using direct numerical simulations coupled with GRI3.0 detailed mechanism. It is shown that both 2-D reaction-diffusion manifold table and 19-step simplified mechanism can describe the temperature and main products accurately, however, for some minor intermediary products, predictions from 2-D reaction-diffusion manifold table is observed to be better than 19-step simplified mechanism. Compared with the 19-step mechanism, 2-D reaction-diffusion manifold table only needs to solve only the transport equations for CO_2 and N_2 species, which greatly simplifies the solution process of chemical reaction and provides a reliable solution for the numerical simulation of turbulence with higher accuracy. This work indicates that as a relatively advanced kinetic simplified method, the reaction-diffusion manifold tabulation method can reduce the computational cost and at the same time retain the accuracy effectively.

Key words: *reaction-diffusion manifold table, direct numerical simulation, triple flames*

Introduction

As a major source of energy, fossil fuels drive the life and production of human society, but also bring a series of exhaust emission problems [1, 2]. We can foresee that this mode of energy supply will still play a dominant role for a long time in future. Therefore, it is of great significance to develop efficient and clean combustion technology. In this point, the design method of numerical simulation has broad prospects [3-5]. In terms of fuel combust mode, perfectly premixed flames and non-premixed flames are the two distinctive forms of combustion, where fuel/oxidizer mixture is thoroughly mixed in the former and separated prior to chemical reaction in the latter. In practical combustors, completely premixed or diffusion flames are hard to achieve, often resulting in partially-premixed flames. The partially-premixed flames have characteristics of both premixed and diffusion flames including *double* [6], *triple* [7], and *edge* [8] flames. They typically contain multiple reaction zones. For instance, a

* Corresponding author, e-mail: pingwang@ujs.edu.cn

double flame contains two reaction zones, a rich premixed zone on the fuel side and a diffusion zone on the oxidant side, while a triple flame includes three reaction zones, two premixed zones and one diffusion zone. These reaction zones are spatially separated but are collectively coupled through thermochemical and hydrodynamic interactions among them. Each reaction zone is affected by other reaction zones, and the global flame structure is strongly dependent on the interactions among these reaction zones [9]. Therefore, there are significant differences among the flame blowout characteristics of partially-premixed flames and those of premixed and non-premixed flames.

As a typical feature that exist in partially-premixed flames, triple flames play an important role in the propagation characteristics of various kinds of flames. Figures 1(a)-1(f) show structure of typical triple flames in various partially-premixed flame configurations [7]. As can be seen in figs. 1(a)-1(f), the curved edge is the unique feature of triple flames formed by the presence of premixed region in the edge. The structure of triple flames was first described by Phillips [10]. Kim *et al.* [11] performed an experimental study to examine the trend of propagation velocity of triple-flames under relatively large mixed fractional gradient. It was found that when the mass fraction gradient becomes larger, the flame propagation velocity gradually decreases, and the propagation velocity of the edge flame was observed to be less than the stoichiometric laminar flame.

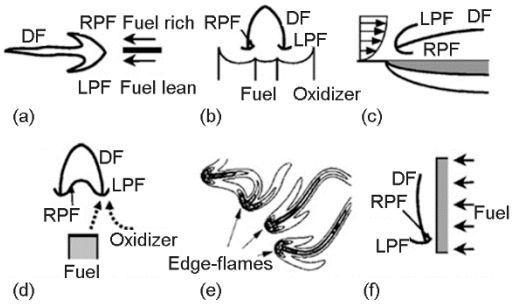

Figure 1. Schematic of triple flames in various flow configurations adapted from [7]; rich premixed flame (RPF), lean premixed flame (LPF), diffusion flame (DF)

The global reaction mechanism is often used in numerical simulations, however, this mechanism hits its limits to describe the structure of triple flames owing to the presence of multiple reaction zones. A more detailed chemical reaction mechanisms were therefore sought. Qin *et al.* [12] studied the effect of gravity on the premixed laminar flame of CH_4-air using an 81-step CH_4 reaction mechanism in the simulation. Yammamoto *et al.* [13] used a 25-step CH_4 chemical reaction mechanism to study the CH_4-air jet triple flames in co-flow condition. Yuan *et al.* [14] analyzed the influence of wall and geometrical structure of flow field on the propagation of CH_4-air triple flames. They have adopted 184 steps CH_4 chemical reaction mechanism to improve the accuracy, however, this has greatly increased the computational time.

In order to reduce the computational cost and effectively improve the calculation accuracy, a number of simplified dynamic methods have been developed in the past few decades, mainly including the path flux analysis method [15], the computational singular perturbation method [16], the in situ adaptive tabulation method [17], and the intrinsic low-dimensional manifolds (ILDM) method [18]. The ILDM method is based on the direct numerical analysis of the dynamic behavior of the chemical system non-linear response. The eigenvalue analysis of the Jacobian matrix of the chemical reaction term is used to decompose the reaction space into a fast reaction subspace and a slow reaction subspace.

The manifold is constructed in a slow reaction subspace to achieve a partial parameter to characterize the composition of the entire chemical system. While ILDM method assumes that the chemical reaction dominates in the process of simplified the mechanism and ignored the influence of convective diffusion on the chemical reaction in the low tem-

perature region. Therefore, it has good simulation accuracy only in the high temperature zone. Increasing the subspace dimension is one of the methods to improve the calculation accuracy of the low temperature zone, but at the same time greatly increases the amount of calculation. The flamelet generation manifolds (FGM) proposed by Oijen *et al.* [19] and the flame prolongation of ILDM (FPI) method proposed by Gicquel *et al.* [20], by adding the influence of flow effects such as diffusion on the basis of the original ILDM method, has been widely used.

After these two methods have been successfully applied to the numerical simulation of premixed and diffusion flame, more and more scientists tried to use it for partially-premixed flames. Fiorina *et al.* [21] applied a 2-D PFI table to a partially premixed flame and found that the PFI model yielded good results when the mixture ratio was in the flammable limits. Once the mixing fraction exceeds the flammable limit, the FPI results do not perform very well. Wu *et al.* [22] simulated the 2-D triple flames, it was found that the predicted mass fraction of CO in the FPI tabulation method was too larger than the detailed reaction mechanism results. Song [23] applied the FGM premixed table and FGM diffusion table to the partially premixed flame by using the flame index concept and obtained a good result, but the cost of simulation gained a lot. Therefore, a new simplified reaction mechanism method was created by Bykov and Maas: reaction-diffusion mainfold (REDIM) method [24]. Wang *et al.* [25] used the 2-D REDIM table combined with the assumed probability density function (PFDF) to calculate the stratified flame used Darmstadt burner, which is in good agreement with the experimental results.

In the present work, we study the combustion characteristics of triple flames under a uniform concentration gradient, and also analyze the ability of 2-D REDIM table to describe the triple flames that exceeds the flammable limit. The GRI3.0 mechanism is used in the parallel triple flames with equivalence ratios in [0, 2] proposed by Wen *et al.* [26]. Further, REDIM tabulation method and 19-step CH_4 chemical reaction mechanism are used to examine the results in order to explore the performance of REDIM table.

The REDIM table

In ILDM method, only the chemical reaction is solved in chemical reaction simulation. However, the REDIM method considers both effect of chemical reaction and molecular transport in process of low-dimensional manifolds generation. The low-dimensional manifold equation [24] is:

$$\frac{\partial \Psi(\theta)}{\partial t} = (I - \Psi_\theta \Psi_\theta^+)\left[F(\Psi) - \frac{d}{\rho} \Psi_{\theta\theta} \circ \text{grad}(\theta) \circ \text{grad}(\theta) \right] \tag{1}$$

where ρ is the density, θ – the local coordinate vector in low-dimensional manifold, x = grad(θ) is the spatial gradient of θ, $\Psi_{\theta\theta}$ – the Hessian matrix, d – the matrix of molecular diffusion coefficients, the sign "$\circ$" is an abbreviation for two vector multiplications with third-order tensors. The process of generating a REDIM table can be divided into following steps [28]:

– Specify initial conditions and boundary conditions of eq. (1).
– Specify the gradient grad(θ) as a function of θ.
– Time integral with eq. (1) until it reaches a stable state.
– Store manifold data, such as Ψ_θ, $\Psi_\theta(\theta)$ $F[\Psi(\theta)]$, *etc.*

In this paper, Dirichlet boundary conditions are used to solve different 1-D laminar flamelet units by INSFLA [27-29] program with GRI3.0 mechanism, then the computational

boundary and initial manifold of the REDIM table are generated. These flamelet units include CH_4-air pure mixing flow, air-pilot counter flow flame and fuel-pilot counter flow flame. As shown in fig. 2(a), the black line on the left indicates the fuel-pilot counter flow flame, the black line on the right indicates the pilot-air counter flow flame, and the black line at the bottom indicates the pure mixing process with no combustion in the CH_4-air counter flow. These lines form the border of 2-D REDIM table. The inner dashed lines indicate the fuel-air counter flow flame at different strain rates and are used to specify the initial manifold of the REDIM table. The strain rates increase with the height of the curves. Too large strain rate can make the flame shut down. The initial manifold can be used to generate the REDIM table as long as it lies inside the borders. Figure 2(b) shows a 3-D framework represented by Y_{N_2}-Y_{CO_2}-Y_{OH}, the green line indicates the instant flame blowout of flamelet unit. It can be seen that the 2-D REDIM table can describe the flame blowout state and it is suitable for simulating partially-premixed flames. The finally convergent file *counterdiff* in INSFLA is imported into REDIM generate program. By specifying the initial conditions and boundary conditions, the initial manifold obtained as shown in fig. 2(c).

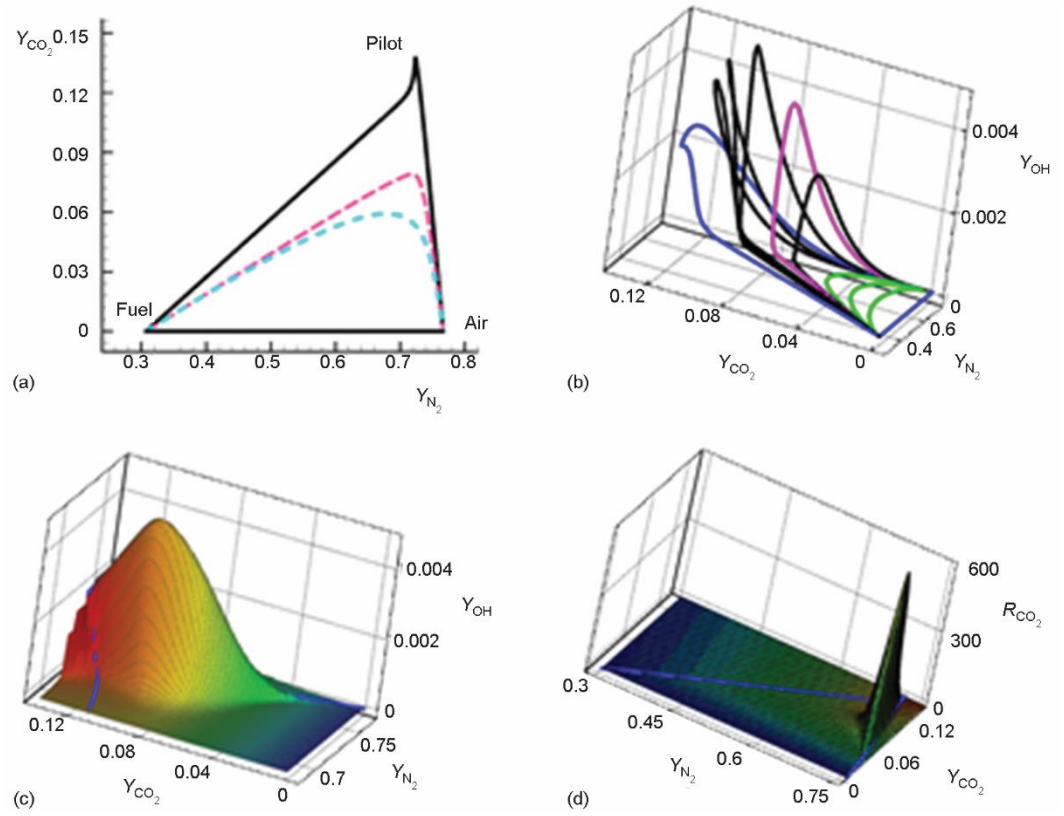

Figure 2. The 2-D REDIM table generation process from beginning to the end

By performing steps 2-4, a 2-D REDIM table with N_2 and CO_2 mass fractions as arguments is finally obtained as shown in fig. 2(d). The Y_{CO_2} characterizes the reaction rate, Y_{N_2}

characterizes the mixing process. Other thermodynamic variables such as CH_4, CO density, temperature, and CO_2 production rate can be obtained by querying the 2-D REDIM table. The value of CO_2 mass fraction as zero corresponds to the pure mixing process and the equivalence ratio, ϕ, have the value of 10 and 0 when the N_2 mass fraction takes the minimum and maximum values, respectively. For the realistic situations, the mass fraction ranges of N_2 and CO_2 can only be located in the area between the two solid blue lines in fig. 2(d).

Computational set-up

Computational domain

Figure 3 shows the inlet conditions that are used in the calculation of laminar triple flames (the Reynolds number is 500). Fresh mixture of methane-air enters the domain from the left at an atmospheric pressure of 1 atm. A uniform inflow velocity of 0.5 m/s is considered along the x-direction, and the concentration gradient changes uniformly along the y-direction from 0 to 15 mm. At the inlet, the equivalent ratio is assumed to increase linearly from 0 to 2, to cover both lean and rich flammable limits, while maintaining the stoichiometric ratio line at the central location in the y direction. Further, to ensure that the triple flames is sufficiently far away from the inlet boundary, the mixture concentration of inlet part is confined to the region of $0 < x < 2$ mm, and the exhaust gas is filled in the region of $2 < x < 25$ mm to ignite unburned gas. Due to the strong variations in flame speed under different equivalence ratios, as the flame propagates along the x-direction, the premixed flame that branches on both the sides gradually bend. As the diffusion effect of the components concentration gradient, the excessive fuel in the rich premixed branch and oxidant in the lean premixed branch are diffused to the middle region. Finally, the triple flames were generated. In the present simulations, we adopt a 2-D rectangular domain of 15 mm (x) × 25 mm (y) and 1000/600 grid cells were set in the x/y directions, respectively, with a uniform cell length of 0.025 mm.

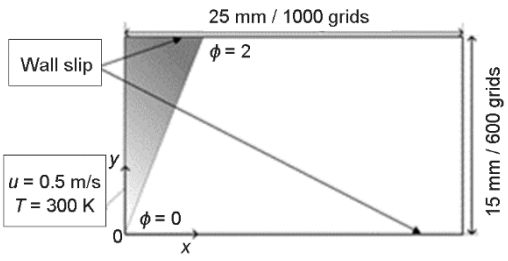

Figure 3. Schematic of the computation domain to simulate triple flames

Numerical set-up

We employed the rho-reacting buoyant foam to do the simulation which solve the reaction in chemkin format. The slip wall is applied at top and bottom boundaries, while the zero-gradient boundary condition is considered at the outlet. For the calculations, a second-order backward scheme is selected for time discretization, a limited difference TVD scheme is adopted for convection term, and a second-order linear Gaussian difference scheme is adopted for diffusion term. In OpenFOAM, the courant number can automatically adjust with the time step, which is set to 0.4 in our cases, and the iteration residual is set to $1 \cdot 10^{-9}$.

Results and discussions

The GRI 3.0 mechanism

Figure 4(a) shows the temperature distribution of the triple flames. The flame temperature rises gradually from the sides (300 K) to the middle area (2100 K). Due to the heat

spread from middle to both sides, the highest temperature is lower over 100 K than the premixed flame at stoichiometric ratio with a temperature of 2226 K. The solid white line in fig. 4(a) is the equivalence ratio contour described by the N_2 mass fraction. The equivalence ratio of the mixture gradually increases along the *y*-direction and the contour bends near the flame front. By combining these contours with the distribution of the OH radicals in fig. 4(c), the position of the rich premixed flame branches and the lean premixed flame branches can be effectively identified.

Figure 4(b) shows a cloud chart of CO_2 reaction rate, where a very light flame branch can be observed in the center location along *y*-direction. This causes excessive fuel on the rich branch side and excess oxidant on the lean branches continues to diffuse in the middle and the mixture is ignited by the high temperature exhaust gas. The lower reaction rate of CO_2 on diffusion flame branch is due to the limited mass fraction of diffusion gas. The diffusion flame branch can be clearly observed in the OH mass fraction cloud map, fig. 4(c). Comparing fig. 4(a), it can be found that OH radicals are ubiquitous in the high temperature zone because fuel is largely decomposed in this zone which generates OH radicals. Due to the presence of the diffusion reaction, the amount of OH radicals is additionally increased, so that the OH radicals are more abundant near the triple-point. Along the branch of the diffusion flame to downstream, the concentration of OH radicals remains constant, as for the two premixed flame branches, the concentration of OH radicals decreases in downstream.

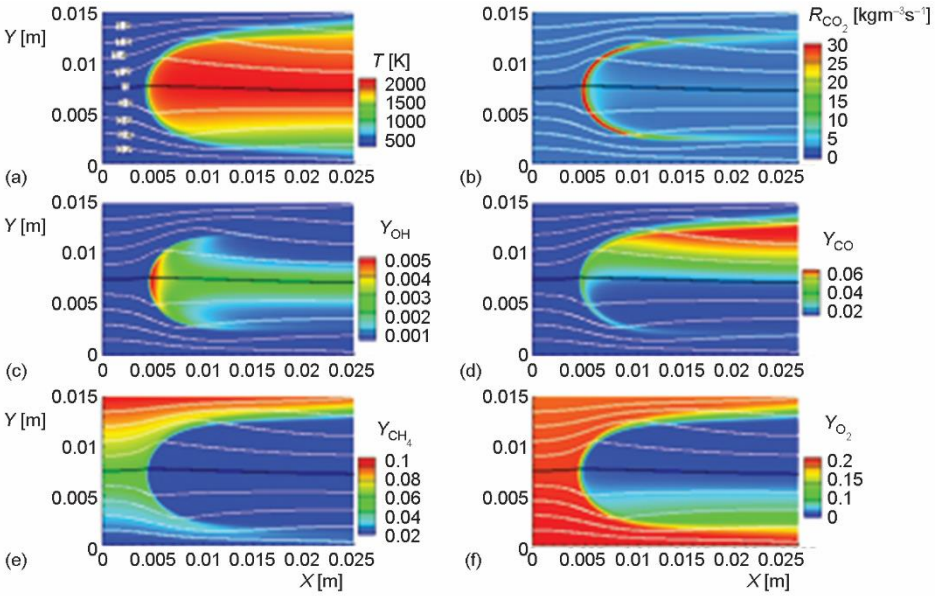

Figure 4. Temperature and main composition information in triple flames, the black bold line represents the position of the stoichiometric ratio, the white solid line represents the equivalence ratio contour

Figure 4(e) shows that a uniform CH_4 concentration gradient is applied to the inlet boundary. Because of diffusion and flame effect, the concentration gradient of CH_4 gradually decreases from upstream to downstream. A large amount of CO products can be found in the rich premixed flame branch, fig. 4(d), with a certain concentration gradient along the

y-direction, because when methane burns, it will break into CO and other small molecular species first [30]. For the lean premixed flame branch, excessive trend to diffuse to rich branch can be seen in fig. 4(f).

Figure 5(a) shows the variations of temperature along *y*-direction at four different axial locations, Δx = 10 mm, 12 mm, 15 mm, and 20 mm away from triple-point, respectively. Observing the temperature distribution at different locations, it was found that along the downstream of the flame, the temperature gradient gradually decreases, which means that the flame thickness increases continuously. Meanwhile, it can be seen in fig. 5(b) that the distribution area of CO_2 reaction rate on the premixed flame branches gradually widens, and the peak value of CO_2 reaction rate decreases to indicate that the chemical reaction rate is significantly reducing along the flame propagation direction. At the downstream locations of the flame, the mass fraction of OH radicals at the diffusion flame branch decreases at first and finally remains constant, fig. 5(c). At the two premixed flame branches, the peak value of OH radicals gradually decreases, and the peak value of OH at lean premixed branch flame is higher than that of the rich premixed flame branch. Meanwhile, two premixed flame branches gradually become blurred. According to Zhang's point [31], most of the OH radicals are generated from O_2 and CH_3 radicals, fig. 5(d).

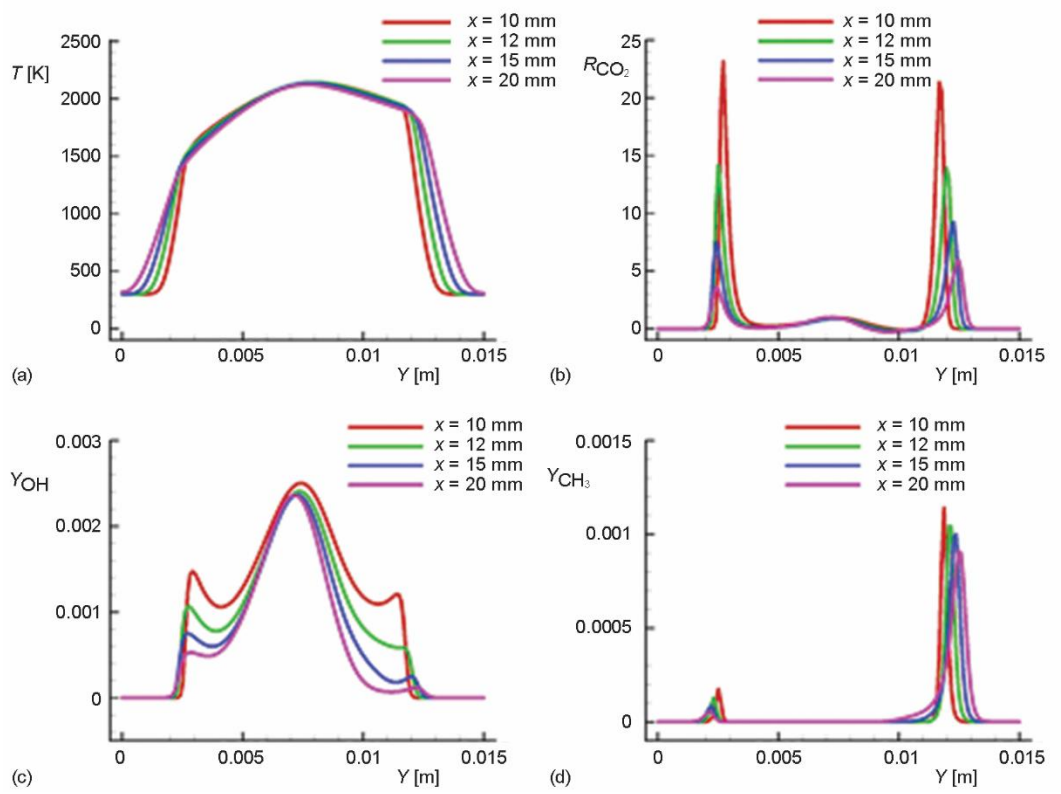

Figure 5. Temperature and mass fractions of components at Δx = 10 mm, 12 mm, 15 mm, and 20 mm away from triple-point

Comparison of REDIM table and 19-step simplified mechanism

In figs. 6(a) and 6(b), we present the results based on GRI 3.0 mechanism as plots of N_2-CO_2-OH mass fraction and N_2-CO_2-T scatter plot distributions respectively. Similarly, figs. 7(a) and 7(b) show the results from the 2-D-REDIM table. For convenient comparison, figs. 7(a) and 7(b) show only a 2-D REDIM table with a N_2 mass fraction in the range of 0.68 to 0.76 (the same equivalent ratio range with GRI 3.0 mechanism calculation). It can be seen that the results from these two methods show almost the same trend, The Y_{N_2}-Y_{CO_2}-Y_{OH} and Y_{N_2}-Y_{CO_2}-T scatter points of triple flames all included in 2-D REDIM table which indicate that the table can be used to solve the triple flames we set in our case.

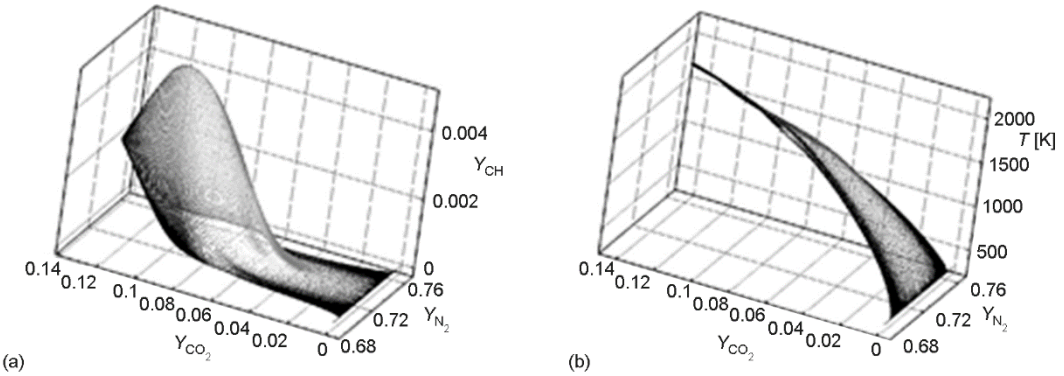

Figure 6. The projection results based on GRI3.0 mechanism

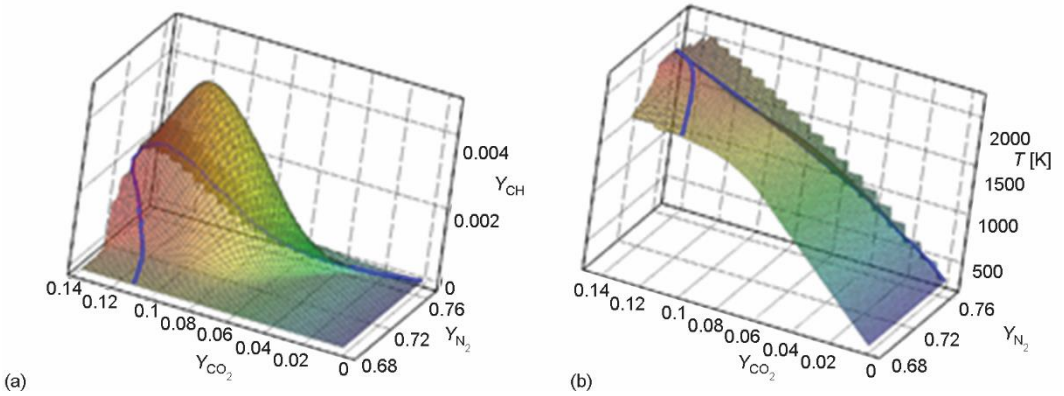

Figure 7. The projection results based on 2-D REDIM table, colored with temperature (300 K, 2100 K)

The results of the triple flames using GRI3.0 mechanism, 2-D REDIM table and 19-step simplified mechanism [32] are shown in fig. 8. It can be seen that the prediction of temperature and main components such as CH_4 and O_2 mass fraction distributions are very similar between GRI3.0 mechanism and 2-D REDIM table. For lean premixed flame branch at downstream, the flame under 2-D REDIM table is little wider than the GRI3.0 results. For CO mass fraction distribution, the results of 2-D REDIM table are very close to the GRI3.0

mechanism in general, in rich premixed flame branch the prediction of mass fraction of CO is smaller than GRI3.0 mechanism, but it is still better than 19-step mechanism. Because 2-D REDIM table method just solved CO_2 and N_2 transport equation, so it runs faster than solving chemical reaction method. In this case (0.6 million cells totally) 2-D REDIM table costs 16 hours while with 19 steps mechanism it costs more than 40 hours. Generate REDIM table only takes a few minutes but preparing flamelet units need a half day. In the study of triple flames, more detailed chemical reaction mechanism can be used to improve the accuracy, but at the higher computation cost.

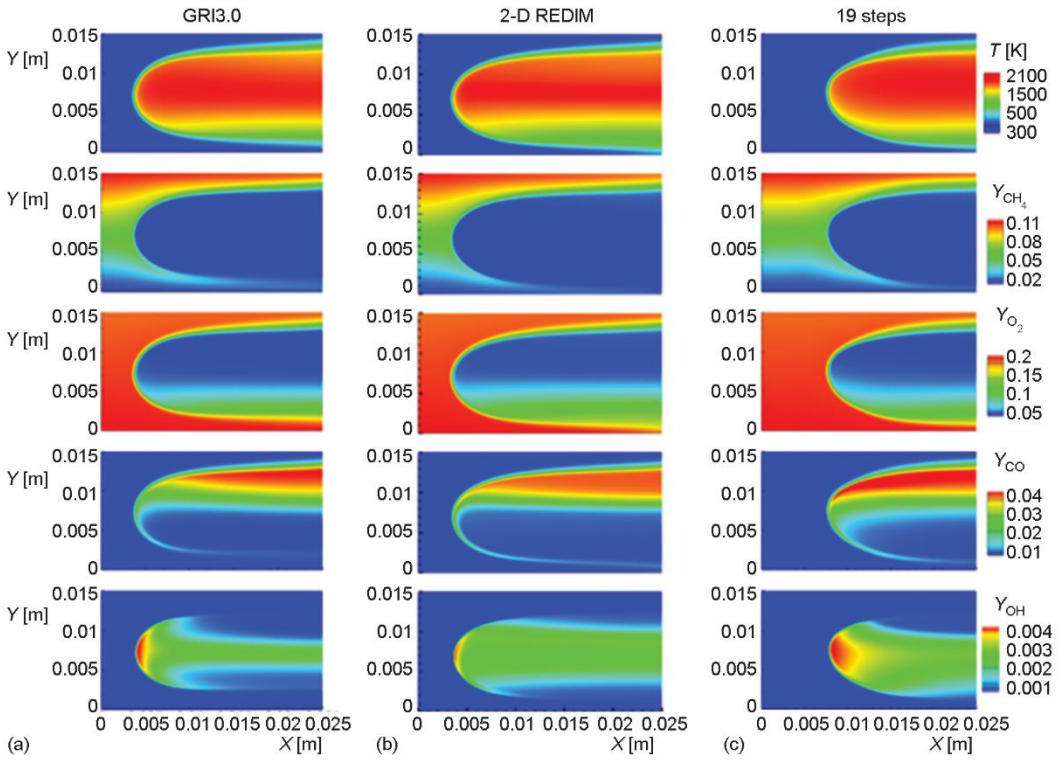

Figure 8. Instantaneous distribution of temperature and component mass fractions based on, (a) GRI3.0 mechanism, (b) 2-D REDIM chemical table, and (c) 19-step mechanism

Figure 9 shows the temperature, CH_4 mass fraction and H_2O mass fraction distribution curves at different locations away from triple-point. The black dots indicate the GRI3.0 mechanism results, the solid curve and dashed curve represent the 2-D REDIM table and 19-step mechanism results, respectively. As can be seen in fig. 9(a), 2-D REDIM table results at different locations are in good agreement with that of the GRI3.0 mechanism. However, in the $3 < y < 7$ mm region, the 2-D REDIM table predicts a lower flame temperature (less than 5% difference) compared to the GRI3.0 mechanism. It is observed that the equivalent ratio in $3 < y < 7$ mm region is approximately between 0.6 and 0.9, which belongs to the lean premixed flame branch. It because few points beyond the 2-D REDIM table borders in this re-

gion, so this part results are processed by mapping method, which may be the main reason for the lower flame temperature in this position.

In other regions, the temperature values of 2-D REDIM table predicts almost same with GRI3.0 mechanism. At two premixed flame branches, the 2-D REDIM table and the 19-step mechanism predict similar temperature gradient with GRI3.0 mechanism, which indicates that 2-D REDIM table and 19-step mechanism can correctly predict the thickness of the premixed flame branches in triple flames. At Δx = 5 mm, the 19-step mechanism results are in good agreement with the GRI3.0 mechanism results, while in Δx = 10 mm and 15 mm, the temperature predicted by the 19-step mechanism is much higher. In fig. 9(b), both 2-D REDIM table and 19-step mechanism agree well with the results of GRI3.0 mechanism in predictions of mass fraction of CH_4. In fig. 9(c), the mass fraction of H_2O in 2-D REDIM table agrees well with the GRI3.0 mechanism at three different locations. However, the results of 2-D REDIM tables are slightly lower than GRI 3.0 mechanism at $3 < y < 7$ mm. By contrast, the 19-step mechanism burns intensely, and the mass fraction of H_2O here is much higher than the actual state.

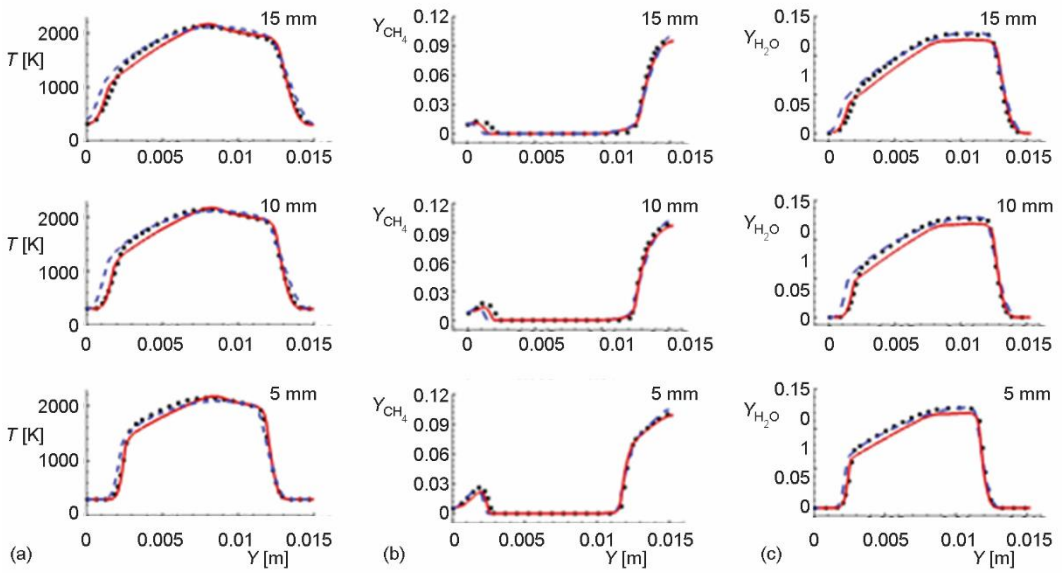

Figure 9. Temperature and mass fractions of CH_4, H_2O distributions at different locations away from the triple-point; • GRI3.0 mechanism, ▬ 2-D REDIM, – – – 19-step mechanism

Conclusions

In this paper, direct numerical simulation was employed to simulate triple flames. Using GRI3.0 mechanism, the flame structure and flow field characteristics were analyzed. A 2-D REDIM table was generated based on GRI3.0 mechanism. To evaluate the performance of the REDIM table, the flames are simulated by using REDIM table and 19-step simplified mechanism. The results indicated that both REDIM table and 19-step simplified mechanism can describe the temperature and main products such as CO_2 and H_2O well, however for some instantaneous products, the 2-D REDIM table has a better performance than 19-step mecha-

nism. As for the deviation of 2-D REDIM table in lean premixed flame branch, it is mainly due to the projection error of boundary points in tabulation, and the accuracy can be improved if the REDIM table boundary is optimized. The calculation boundary considered in generating 2-D REDIM table is comprehensive, so it can be directly applied to other complex turbulent flame. The REDIM table greatly simplifies the process of solving chemical reactions, which can reduce the dependence on computing resources, at the same time, the calculation accuracy is guaranteed effectively, which provides a reliable solution for numerical simulation of turbulence simulation.

Acknowledgment

The support of Natural Science Foundation of China through project 91741117 and 51576092, and the support of PAPD project funded by Jiangsu Higher Education Institution are gratefully acknowledged. The authors also thank Prof. U. Maas and his team (Karlsruhe Institute of Technology, Germany) for providing the code for generating REDIM chemistry table. The support of High-Tech Research Key laboratory of Zhenjiang (SS2018002) is also appreciated.

References

[1] Fabienne, C., *et al.*, Applications of Oxygen for NOx Control and CO_2 Capture in Coal-Fired Power Plants, *Thermal Science*, *10* (2006), 3, pp. 119-142
[2] Kegl, B., *et al.*, Influence of Biodiesel on Injection, Fuel Spray, and Engine Characteristics, *Thermal Science*, *12* (2008), 2, pp. 171-182
[3] Nemoda, S., *et al.*, Numerical Simulation of Porous Burners and Hole Plate Surface Burners, *Thermal Science*, *8* (2004), 1, pp. 3-17
[4] Jebamani, D., Kumar, T., Studies on Variable Swirl Intake System for DI Diesel Engine Using Computational Fluid Dynamics, *Thermal Science*, *12* (2008), 1, pp. 25-32
[5] He, Z., X., *et al.*, A Numerical Study of the Effects of Injection Rate Shape on Combustion and Emission of Diesel Engines, *Thermal Science*, *18* (2014), 1, pp. 67-78
[6] Li, C., *et al.*, Stabilization of Double Flames Interacting with the Intersecting Flow on a V-Shaped Burner, *Combustion Science and Technology*, *184* (2012), 12, pp. 2117-2135.
[7] Azzoni, *et al.*, The Structure of Triple Flames Stabilized on a Slot Burner, *Combustion & Flame*, *119* (1998), 1-2, pp. 23-40
[8] Kurdyumov, V. N., *et al.*, Dynamics of an Edge Flame in a Mixing Layer, *Combustion and Flame*, *139* (2004), 4, pp. 329-339
[9] Aggarwal, S., K., Extinction of Laminar Partially Premixed Flames, *Progress in Energy & Combustion Science*, *35* (2009), 6, pp. 528-570
[10] Phillips, H., Flame in a Buoyant Methane Layer, *Symposium on Combustion*, *10* (1965), 1, pp. 1277-1283
[11] Kim, M. K., *et al.*, Effect of Velocity Gradient on Propagation Speed of Tribrachial Flames in Laminar Coflow Jets, *Proceedings of the Combustion Institute*, *31* (2007), 1, pp. 901-908
[12] Qin, X., *et al.*, Gravity, Radiation, and Coflow Effects on Partially Premixed Flames, *Physics of Fluids*, *16* (2004), 8, pp. 2963-2974
[13] Yammamoto, K., *et al.*, Behaviors of Tribrachial Edge Flames and Their Interactions in a Triple-Port Burner, *Combustion and Flame*, *162* (2015), 5, pp. 1653-1659
[14] Yuan, Ye., *et al.*, Numerical Study of the Effects of the Channel and Nozzle Wall on the Transition Behavior of a Methane Tribrachial Flame in a Confined Flow, *Fuel*, *160* (2015), Nov., pp. 366-374
[15] Li, S. L., *et al.*, The Generation of a Reduced Mechanism for Flame Inhibition by Phosphorus Containing Compounds Based on Path Flux Analysis Method, *Chinese Journal of Chemical Engineering*, *21* (2013), 4, pp. 357-365
[16] Lam, S. H., Using CSP to Understand Complex Chemical Kinetics, *Combustion Science and Technology*, *89* (1993), 5-6, pp. 375-404

[17] Lu, L. Y., *et al.*, Computationally Efficient Implementation of Combustion Chemistry in Parallel PDF Calculations, *Journal of Computational Physics*, *228* (2009), 15, pp. 5490-5525
[18] Maas, U., Pope, S. B., Implementation of Simplified Chemical Kinetics Based on Intrinsic Low-Dimensional Manifolds, *Symposium on Combustion*, *24* (1992), 1, pp. 103-112
[19] Oijen, J. A., *et al.*, Modeling of Complex Premixed Burner Systems by Using Flamelet-Generated Manifolds, *Combustion and Flame*, *127* (2001), 3, pp. 2124-2134
[20] Gicquel, O., *et al.*, Laminar Premixed Hydrogen/Air Counterflow Flame Simulations Using Flame Prolongation of ILDM with Differential Diffusion, *Proceedings of the Combustion Institute*, *28* (2000), 2, pp. 1901-1908
[21] Fiorina, B., *et al.*, Approximating the Chemical Structure of Partially Premixed and Diffusion Counterflow Flames Using FPI Flamelet Tabulation, *Combustion and Flame*, *140* (2005), 3, pp. 147-160
[22] Wu, H., *et al.*, A Pareto-Efficient Combustion Framework with Submodel Assignment for Predicting Complex Flame Configurations, *Combustion and Flame*, *162* (2015), 11, pp. 4208-4230
[23] Song, S., Large Eddy Simulation of Multi-Modal Turbulent Combustion Based on FGM, M. Sc. thesis, Zhejiang University, China, 2014
[24] Steinhilber, G., Maas, U., Reaction-Diffusion Manifolds for Unconfined, Lean Premixed, Piloted, Turbulent Methane/Air Systems, *Proceedings of the Combustion Institute*, *34* (2013), 1, pp. 217-224
[25] Wang, C., *et al.*, Sub-Grid Scale Combustion Model Based on REDIM Method and Its Application, *CIESC Journal*, *66* (2015), 12, pp. 4948-4959
[26] Nguyen, P. D., *et al.*, Multidimensional Flamelet-Generated Manifolds for Partially Premixed Combustion, *Combustion and Flame*, *157* (2010), 1, pp. 43-61
[27] Razus, D., *et al.*, Experimental and Computed Burning Velocities of Propane-Air Mixtures, *Energy Conversion and Management*, *51* (2010), 12, pp. 2979-2984
[28] Kuznetsov, M., *et al.*, Laminar Burning Velocities of Hydrogen-Oxygen-Steam Mixtures at Elevated Temperatures and Pressures, *Proceedings of the Combustion Institute*, *33* (2011), 1, pp. 895-903
[29] Szabo, T., *et al.*, Parameterization of Laminar Burning Velocity Dependence on Pressure and Temperature in Hydrogen/Air/Steam Mixtures, *Combustion Science and Technology*, *184* (2012), 10-11, pp. 1427-1444
[30] Suresh, K., *et al.* Flame Structure Interactions and State Relationships in an Unsteady Partially Premixed Flame, *AIAA Journal*, *36* (1998), 7, pp. 1190-1199
[31] Zhang, L., *et al.*, Measurement and Analysis of 1-D OH Radicals Absolute Concentration in Flat Flame, *Journal of Combustion Science and Technology*, *23* (2017), 2, pp. 161-165
[32] Toshimitsu, K., *et al.*, Numerical Simulations and Planar Laser-Induced Fluorescence Imaging Results of Hypersonic Reactive Flow, *Journal of Propulsion and Power*, *16* (2000), 1, pp. 16-21

Paper submitted: September 9, 2019
Paper revised: June 17, 2020
Paper accepted: June 19, 2020